ASSESSMENT OF PELLET INJECTION FOR NET
PART III

Uncertainties Inherent in Present Ablation Models

L. L. Lengyel

IPP 1/232 September 1984

MAX-PLANCK-INSTITUT FÜR PLASMAPHYSIK

8046 GARCHING BEI MÜNCHEN

MAX-PLANCK-INSTITUT FÜR PLASMAPHYSIK

GARCHING BEI MÜNCHEN

ASSESSMENT OF PELLET INJECTION FOR NET
PART III

Uncertainties Inherent in Present Ablation Models

L. L. Lengyel

IPP 1/232 September 1984

Die nachstehende Arbeit wurde im Rahmen des Vertrages zwischen dem Max-Planck-Institut für Plasmaphysik und der Europäischen Atomgemeinschaft über die Zusammenarbeit auf dem Gebiete der Plasmaphysik durchgeführt.

IPP 1/232 L.L. Lengyel

ASSESSMENT OF PELLET INJECTION FOR NET, PART III:

Uncertainties Inherent in Present Ablation Models

Abstract

Existing ablation models yield acceptable results for thermal plasmas at low and intermediate temperatures. Care should be exercised in extrapolating these results to thermonuclear plasmas because of the limitations inherent in these models:

(i) the neglect in the energy transport of the spectrum of stopping lengths or penetration depths corresponding to different energy carrier species and to different energy groups of a single species;

(ii) the neglect of the change of the initially spherical expansion of the pellet substance into channel flow along magnetic surfaces and the associated changes in gasdynamic and magnetic shielding;

(iii) the neglect of parallel (to the magnetic field) heat conduction effects.

Uncertainties Inherent in Present Ablation Models

We shall start with a brief review of what is known about the physics of pellet ablation and subsequently measure the ablation models against this state of knowledge.

1. Pellet Ablation

1.1 Energy transfer to the pellet

A pellet injected into a plasma is exposed to bombardment by thermal and non-thermal particles present in the recipient plasma. In fusion devices of interest, thermal electrons, neutral-beam-produced ions, alpha particles, and, in certain discharges, runaway electrons may serve as energy carriers. The effect of thermal ions may be neglected as long as electrostatic shielding remains negligible. In the presence of a magnetic field, the particle fluxes incident at the pellet surface may be anisotropic: plasma particles with gyro-radii of the order of the pellet dimension (thermal electrons and ions) pierce the pellet or the high-density gas cloud surrounding it while moving along the magnetic field lines, whereas particles of large gyro-radii (e.g. alpha particles) may strike the pellet from all directions. The particles penetrating the pellet or its gas mantle suffer collisions, thus transferring their energy, partially or totally, to the pellet substance. The penetration depths and thus the energy deposition profile are functions of the incident particle energy. As is know, in the case of thermalized particles with a half Maxwellian energy distribution, the main part of the energy flux is carried by a relatively small number of particles of the high-energy tail of the distribution function. These particles may penetrate the ablatant appreciably deeper than those having the average (thermal) energy of the plasma. The ablation, i.e. the removal of subsequent molecular layers from the pellet surface, is a result of the simultaneous action of particle groups of different energies penetrating to different depths in the gas mantle and in the pellet itself. The same is true of the case when different energy

carrier species, each with its own distribution function, are present in the plasma. Simultaneous energy deposition at different depths defines the rate of pellet ablation and the course of expansion of the ablated substance. Consequently, the build-up and effectiveness of a shielding layer around the pellet, as discussed in the next section, are functions of the species present in the recipient plasma and at the energy distribution functions of each of them.

1.2 Ablation hydrodynamics

Pellet particles are removed from the pellet surface as soon as the energy transferred to them exceeds their binding energy (approx. 0.005 eV per atom for hydrogen isotopes). A dense and relatively cold gas cloud forms around the pellet and intercepts most of the incident plasma particles. The pressure (i.e. energy per unit volume) may temporarily be much larger in this cloud than in the background plasma. The high-density cold gas mantle may act as a transient energy accumulator: the energy input rate to the cloud is determined by the directed or thermal velocities of the incident energy carriers (thermal electrons or non-thermal particles), whereas the energy removal rate is defined by the local expansion velocity of the cold pellet particles. As a result of the large pressure gradients developed, the particles removed from the pellet surface are accelerated away from it. At the same time, hydrodynamic shocks may penetrate and preheat the pellet. The expansion of the pellet substance remains approximately spherically symmetric (depending upon the symmetry of the incident energy flux) as long as the bulk of the expanding gas is not ionized and does not interact with the magnetic field.

In this initial phase, the pellet ablation and the expansion dynamics depend primarily on the heat deposition profile in the pellet substance, e.g. on the penetration depths of the different energy carrier species present in the plasma (thermal and non-thermal electrons and ions, alpha particles, each with their own distribution function).

As the expansion proceeds, pellet particles undergo collisions with plasma particles and become ionized. Two alternative processes may take place: direct ionization followed by dissociative recombination or dissociation and subsequent ionization. The ionized pellet particles interact with the magnetic field. This interaction is manifested in two major effects:
(a) gradual deceleration and stopping of the transverse motion of the ionized pellet substance and its "funnelling" into magnetic flux tubes, i.e. the conversion of an initially spherically symmetric motion into an approximately linear channel flow;
(b) "stretching" of the magnetic field lines by the decelerating pellet plasma. The degree of the magnetic field distortion (up to complete expulsion of the magnetic field lines from the pellet substance) depends on the energy density of the pellet substance and on the magnetic field strength, i.e. on the beta ratio. A third effect, specific to toroidal magnetic field configurations with non-uniform field distributions, is the radial drift of the ionized high-beta pellet substance.

The conversion of the initially spherically symmetric expansion into an approximately 1-D channel flow may cause a temporary pile-up of the pellet substance in the transition zone, thus plugging the entrance region of the channel and resulting in a significant increase of the gasdynamic shielding of the pellet against the incident energy flux carried by particles moving with sufficiently small gyro-radii along the magnetic field lines. Diffusion across the field lines, of course, modifies the 1-D channel flow picture, but the transverse diffusion rate is expected to be much smaller than the axial velocity of the particles. According to experimental observations /14,16/ to H_α radiation traces in particular, the pellet substance expands preferentially along the magnetic field lines. Transition from spherical expansion to a linear channel flow thus seems to be the dominant flow process for at least the first phase of the pellet substance expansion.

The expulsion of the magnetic field lines from the pellet substance reduces the incident flux of those energy carriers that are confined to magnetic field lines (i.e. particles with sufficiently small gyro radii).

2. Ablation Models

2.1 Calculation of the energy flux affecting the pellet surface

In the published ablation calculations, thermal electrons of a single (average) temperature are considered to be the only energy carriers. The energy deposition rate has been determined by calculating the energy depletion of a monoenergetic beam of test particles. (The method was originally proposed by Gralnick /1/ and in a refined form by Parks et al. /2/. See also Parks and Turnball /3/, or Milora and Foster /4/.) According to /3/,

$$\frac{dE_e}{dx} = n_a L(E_e) \tag{1}$$

$$\frac{dQ_e}{dx} = n_a Q_e \left(\sigma_T(E_e) + 2\frac{L(E_e)}{E_e} \right) \tag{2}$$

where E_e and Q_e denote the electron energy and energy flux carried by the electrons, n_a is the neutral particle density, σ_T and L are the effective back-scattering cross-section and the energy loss function of the incident electrons in the neutral gas specified.

Thermal conduction effects have been neglected in all neutral gas shielding approximations. It was shown in /5/ that the temperature gradients obtained in this (hydrodynamic) approximation at the pellet surface yield conduction flux values comparable with those stemming from eqs. (1) and (2), i.e. the neglect of thermal conductivity is a posteriori not justified.

It should be noted, however, that the inclusion of the usual thermal conduction term would not necessarily automatically resolve the

inconsistency. Indeed, the assumption of local thermal conduction is only valid if the mean free path of the energy carriers is sufficiently small, compared with the gradient length. In the opposite case, hot electrons residing in the high-temperature wing of the gradient may transport energy to the cold region even though the conduction flux based on the local temperature values is negligible there. To prove this point, calculations were performed /6/, in which a linear channel geometry was assumed, with a high-density cold gas residing at the left boundary and a high-temperature plasma in the rest of the channel (see Fig. 1). From each station x of the channel test particles were "launched" in the direction of the cold gas, starting with the local (thermal) electron temperature $T_e(x)$ and density $n_e(x)$ values. The initial flux and energy of the test particles is thus given by $\Gamma_e(x) = \frac{1}{4} n_e(x) v_{eth}(x)$ and $E_e(x) = 2kT_e(x)$. While traversing the colder region, the flux and energy of the test particles reduce according to the expressions

$$\Gamma_e(x') = \Gamma_e(x) - \int_x^{x'} \left(\partial \Gamma_e / \partial x\right) dx'' , \qquad (3)$$

$$E_e(x') = E_e(x) - \int_x^{x'} \left(\partial E_e / \partial x\right) dx'' .$$

The energy flux carried by these particles can be calculated at any intermediate station as

$$Q_e(x') = \Gamma_e(x') E_e(x') . \qquad (4)$$

The collision terms defining the flux and energy reduction rates were given in the form

$$\frac{d\Gamma_e}{dx} = -\Gamma_e \left(n_a \sigma_{ea} + n_e \sigma_{ei} \right), \qquad (5)$$

$$\frac{dE_e}{dx} = -\left[2 n_a L(E_e) + \frac{3}{2} \frac{m_e}{m_a} (E_e - E_i) n_e \sigma_{ei} \right]$$

where the collision cross-sections and the loss function were calculated as functions of the test particle energy. Let us denote the flux and energy of the test particles arriving at the $x = 0$ left boundary by asterisk ($*$). These quantities are functions of the station x at which the test particles were launched. The values of $\Gamma_e^*(x)$ and $Q_e^*(x)$ are shown in Fig. 1b as functions of the x coordinate. The curves correspond to the n_a, n_e, T_a, and T_e distributions shown in the same figure ($T_i = T_a$). As can be seen, electrons residing in the high-temperature wing of the gradient (thus not necessarily those of the undisturbed plasma) may contribute more to the energy flux at $x = 0$ than those residing closer to the origin of the coordinate system (and, as a matter of fact, more than the electrons of the undisturbed hot plasma). Electron-ion collisions were found in these calculations to be as important as electron-neutral collisions.

Figure 2 is a plot of the electron mean free path length and of the ratio of classical conduction (Spitzer-Harm) and free flux limit heat flux values. The corresponding electron temperature and density distributions are shown in the same figure. As can be seen, in the low-density high-temperature wing of the gradient, the mean free path is considerably larger than the gradient length, even for thermal particles. The Spitzer-Harm conductive flux value exceeds the free flux limit by a factor of 4 in this region.

Another disputable point in the neutral shielding ablation models is the assumption of monoenergetic particle beams in the context of eqs. (1) and (2). The energy deposition profile obtainable by integrating these equations over the temperature range of a Maxwellian (or any other) energy distribution may be quite different from that corresponding to an average energy. Different particle energies mean different spatial deposition bands and thus modification of the ablation dynamics. Figure 3 shows the location of the deposition bands for a given neutral density distribution and three different beam energies /7/. This effect may gain particular relevance if various energy carriers, thermal and non-thermal, are

present in a plasma. No calculations accounting for these phenomena have yet been performed.

2.2 Neutral shielding approximation

As can be seen from eq. (1.1), the depletion of the electron energy is defined by the line density integral

$$\int_{E_{e0}}^{E_{ep}} dE_e / L(E_e) = \int_{\infty}^{r_p} n_a \, dr \,, \qquad (6)$$

where subscripts p and o (or ∞) correspond to the pellet surface and undisturbed plasma, respectively. In all neutral gas shielding approximations available, the neutral density distribution appearing in (6) is calculated by means of 1D spherical gasdynamic expansion models. However, as has been discussed in Sec. 1.2, the initially spherical flow is funnelled into flux tubes along the toroidal magnetic field. The temporal variation of the line integral (6) and thus of the thickness of the shielding layer should be different in funnelled flows than in the spherical expansion models used.

To check this ansatz, computations were made with a channel flow gasdynamic code which has a cold particle source at the left-hand boundary and fully takes the ionization dynamics into account. The strength of the particle source was calculated from the local electron density and electron temperature values by means of the neutral shielding model /3/. The channel cross-section (constant area) and the channel length, i.e. the size of the plasma reservoir, were prescribed (input parameters estimated from the observed cross-sections of ablation clouds and the length of toroidal flux tubes). As can be seen from Fig. 4, as a result of the pile-up of the high-density shielding mass in the inlet section of the channel, the ablation rate rapidly decreases (i.e. within the residence time of the pellet in the flux tube) from its initial value to a fraction of the value resulting from the spherical neutral gas shielding model. Of course, the exact value of the effective flux tube cross-section is not known and the effect of cross-field diffusion was neglected. Nevertheless, the obvious difference between the spherical expansion result and the asymptotic value resulting from linear expansion warrant care in calculations of this kind.

2.3 Magnetic shielding

The phenomenon and implications of magnetic shielding have been discussed in Sec. 1.2. The available neutral shielding models are based on spherical gasdynamic expansion in the absence of any magnetic field and thus cannot account for the phenomena discussed. Various attempts have been made to estimate the relevance of magnetic shielding, starting with Rose's balloon model /8/, in which it was assumed that the ablated material instantaneously ionizes and expands by blowing a diamagnetic balloon around the pellet. Chang /9/ allowed for partial penetration of the magnetic field into the pellet substance and analyzed the corresponding nozzle flow in a magnetic flux tube of variable cross-section with the help of a set of conservation equations.

It was shown in /10/ that the magnetic Reynolds number based on the cloud parameters surrounding the pellet $R_m = \sigma \mu_0 v \Delta r$ plays a decisive role in defining the rate of convection of the magnetic field lines away from the pellet and their re-diffusion, i.e. the magnitude of magnetic shielding. Parks /11/ calculated the distortion of a magnetic field near a pellet by prescribing a certain velocity distribution and considering the above-mentioned two processes. An expression was proposed in /10/ for estimating the energy flux reduction factor η caused by magnetic shielding (by taking only thermal electrons into account): $\eta = \eta(r_p, r_I, r_{ec}, R_m)$, where r_p, r_I, r_{ec} and R_m denote the pellet radius, ionization radius, electron gyro-radius, and magnetic Reynolds number, respectively. The estimated values of η were found to lie between 0.1 and 0.5, depending on the plasma parameters assumed. It should be noted that none of the existing magnetic shielding approximations and estimates represent a self-consistent treatment of the electromagnetic - hydrodynamic problem. The real magnitude of magnetic shielding could only be determined by means of (at least) 2D calculations based on the simultaneous solution of Maxwell's equations and the gasdynamic equations. In 1D calculations, correction factors such as η may be used as an approximation.

3. Experiments

Numerous experimental data are available on pellet injection in tokamak discharges. Best documented are the data obtained on ISX-B /12/ and PDX /13/. A rather useful and informative source work on pellet fuelling experiments as well as on the comparison of ablation theory with measurements based on ISX-B results is /14/. The experiments reported were performed at electron temperatures 0.8 keV to 1.1 keV and electron densities 10^{19} m^{-3} to 3 x 10^{19} m^{-3} ($T_e(o) \approx$ 0.8 keV, $n_e(o) \approx$ 2 x 10^{19} m^{-3} in the case of PDX) with or without NB injection. The relevant observations gathered in these experiments are briefly summarized here.

(a) The emission of H_α radiation seems to yield a reliable measure of the ablation rate (a systematic comparison with line density measurements performed in ISX-B has been given in /14/). Besides information on the ablation rate, H_α measurements provide information on the size and preferential direction of expansion of the partially ionized ablatant.

(b) As has been reported, pellet ablation in ohmic discharges of low and intermediate temperatures and intermediate densities can be fairly well described in terms of the neutral shielding model, in spite of some relevant differences between observations and the basic assumptions of the model. These differences are as follows:

(b1) A nearly periodic, and usually large-scale, oscillation has been observed in the H_α emission. Correlation between the observed H_α emission oscillations and the appearance of bright streaks along the magnetic field lines was reported in /14/. The origin of these oscillations is not yet clear. They might be caused (i) by a periodic blow-off of the shielding gas cloud, i.e. by gasdynamic oscillations, or (ii) by the passage of the pellet over rational and irrational magnetic flux surfaces and the associated variation of the energy flux incident on the pellet, or (iii) by irregular pellet shape and/or irregular (tumbling) pellet motion along the flight path.

On the basis of (b1), a definite correlation between the location of the rational magnetic surfaces and the bright streaks in the radial H_α distribution was proposed by Büchl /15/.

(b2) An impediment of the ablatant flow perpendicular to the magnetic field was reported in /14/ on the basis of H_α emission and interferometric measurements. The funnelling of the flow in magnetic flux tubes may explain the periodic bright streaks reported in /14/ and /15/.

(c) A statistical evaluation of the ISX-B pellet experiments was given in /14/ both for "low" ($\sim 10^{19}$ m^{-3}) and"high"($\sim 3x10^{19}m^{-3}$) densities. The results (figs. 5.7 to 5.9 of /14/) demonstrate that, although neutral shielding theory may yield, on the whole, acceptable results, the ablation details, i.e. the time evolution of the shielding dynamics, cannot be reproduced by this model; this makes the extrapolaribility of the corresponding results rather uncertain.

(d) The neutral shielding model does not yield correct results if non-thermal particles such as runaway electrons or NB ions are present in the plasma. In the case of runaways, a volumetric expansion or "blow-up" of the pellet has been observed (shadowgraphs and interferograms reported in /14/). Apparently, runaways penetrating or traversing the pellet cause a process that is different from the usual surface ablation. The same holds probably for other non-thermal particles as well, provided their penetration depths appreciably differ from that of thermal particles.

(e) At elevated plasma temperatures, the observed ablation rates are up to an order of magnitude smaller than those calculated with the neutral shielding model /14/. It is believed that at higher temperatures magnetic shielding (partial expulsion of the magnetic field lines from the ablated substance and funnelling the flow in toroidal flux tubes) play an increased role.

(f) Unexpectedly high ionization degrees have been measured interferometrically in the ablation cloud: apprx. 20 % with $ne_{max} \gtrsim 10^{26}$ m^{-3} /14/. The presence of neutral particles has not been taken into account in these interferograms.

(g) There are a number of observations that may not have anything to do directly with pellet ablation, but are worth mentioning from the point of view of pellet-plasma interaction (i.e. indirect effect on the ablation rate). Such observations are as follows /12, 13/:

g.1 If MHD activities are present in the recipient plasma (Mirnov oscillations), the ablation rate is reduced.

g.2 If saw-tooth oscillations are present in ohmic discharges, they are damped by the ablated substance.

g.3 In NB-heated plasma, if MHD activities are present, they are damped by the pellet. At the same time, saw-tooth oscillations may be excited.

g.4 With regard to the pellet penetration depth: shallow penetration may cause large sustained increase of Mirnov oscillations. Intermediate penetration may cause central current peaking and appearance of saw-tooth oscillations. Deep penetration was observed to cause from time to time short bursts of large-amplitude Mirnov oscillations.

g.5 The local plasma parameters such as electron temperature and electron density may suffer almost instantaneous changes at locations far from the site of pellet ablation (more correctly: from the site of visible H_α emission). The cause of this phenomenon is not yet clear: either particles are deposited in regions far from the H_α emission, or part of the ablated and ionized particles diffuse at anomalously high rates. The observed local charge exchange intensity

does not seem to be sufficient to explain the sizable particle transport.

4. Conclusions

(a) The existing neutral shielding ablation models yield results that agree, within tolerable limits, with the majority of measurements performed at low and intermediate plasma temperatures.

(b) Care should be exercised in extrapolating these results to thermonuclear plasma conditions because of at least two major limitations inherent in these models:

(b.1) limitation of the energy transport to the pellet to transport by monoenergetic particles (thermal electrons), and neglect of the spectrum of stopping lengths and penetration depths corresponding to different energy carrier species and to different energy groups of a single species.

(b.2) The neglect of magnetic shielding effects manifested in the change of the initially spherical expansion of the pellet substance into channel flow along magnetic flux surfaces (i.e. the change of the gasdynamic shielding efficiency) and in the partial expulsion of the magnetic flux lines from the pellet substance and the corresponding reduction of the incident particle and energy fluxes affecting the pellet.

An ablation model applicable to thermonuclear plasmas should provide reliable approximations to these two major phenomena.

Acknowledgement

Useful discussions with K. Borrass, F. Engelmann, M. Kaufmann, K. Lackner and W. Schneider are acknowledged. The numerical model used for channel flow calculations has been developed in cooperation with W. Schneider.

References

/1/ S.L. Gralnick, Nucl. Fusion 13 (1973), 703

/2/ P.B. Parks, R.J. Turnball, and C.A. Foster, Nucl. Fusion 17 (1977), 539

/3/ P.B. Parks and R.J. Turnball, Phys. Fluids 21 (1978) 1735

/4/ S.L. Milora and C.A. Foster, IEEE Trans. Plasma Sci. 6, (1978), 578

/5/ L.L. Lengyel, Phys. Fluids 23 (1980, 656

/6/ M. Kaufmann, K. Lackner, L. Lengyel, and W. Schneider, Verhandl. DPG (VI), 19 (1984), 1210

/7/ L.L. Lengyel and D.F. Düchs, Proc. 10th Symp. Fusion Technology, Padua 1978, Vol. 1 (1979) 283

/8/ D.J. Rose, Techn. Div. Memo No. 82, Culham, 1968; see also P.A. Politzer and C.E. Thomas, Pric. Fusion Fuelling Workshop, Princeton, 1977

/9/ C.T. Chang, Nucl. Fusion 15 (1975), 595

/10/ L.L. Lengyel, Phys. Fluids 21 (1978), 1945

/11/ P.B. Parks, Nucl. Fusion 20 (1980), 311

/12/ S.L. Milora et al., Nucl. Fusion 20 (1980), 1491

/13/ S.L. Milora et al., Nucl. Fusion 22 (1982), 1263

/14/ C.E. Thomas, ORNL/TM-7486, Oak Ridge Nat.Lab., 1981

/15/ K. Büchl and E. Oberlander, May-Planck-Inst.f.Plasmaphysik, Annual Rept. 1983, p. 39.

/16/ K. Büchl, Verhandl. DPG (VI), 18 (1983), 429

Effect of non-local thermal transport

Fig.1

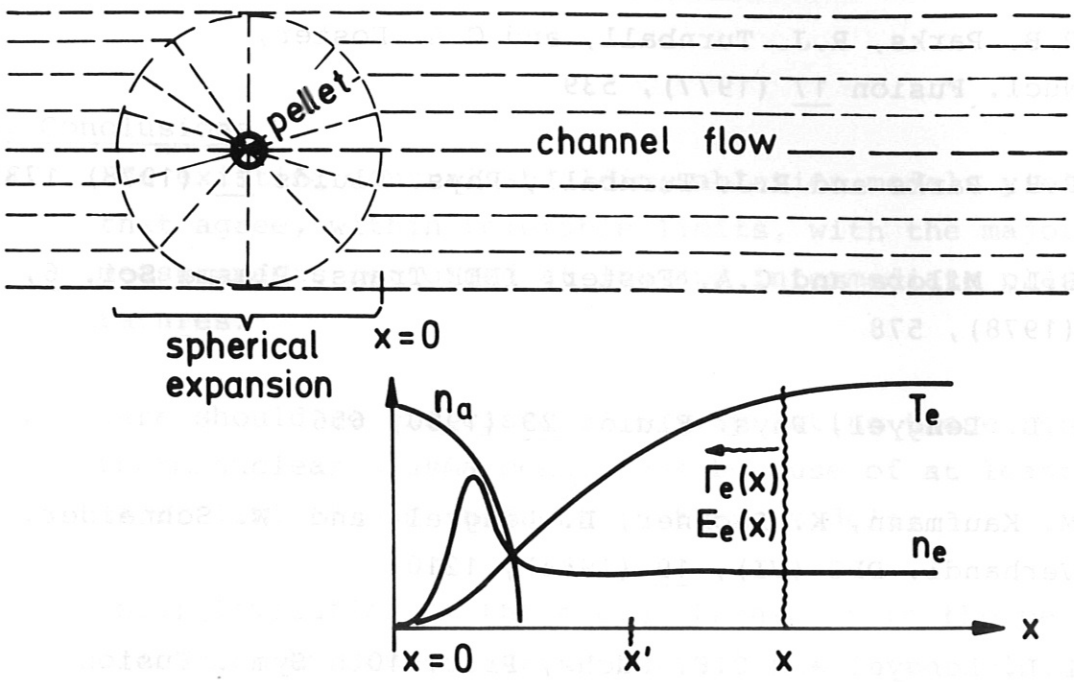

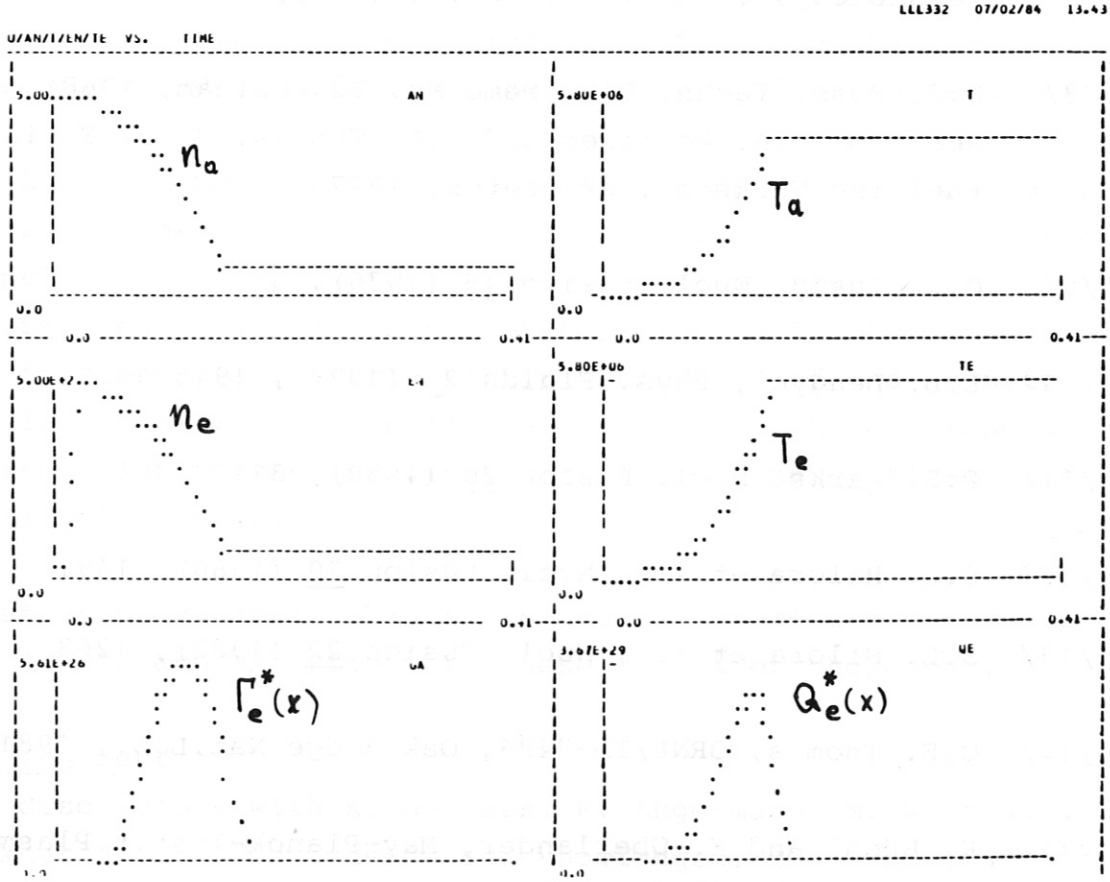

Fig.2: Electron mean free path length λ_E and heat flux ratio q_{SH}/q_{FL} (Spitzer-Haerm and free flux limit) profiles for the momentary n_e and T_e distributions shown.

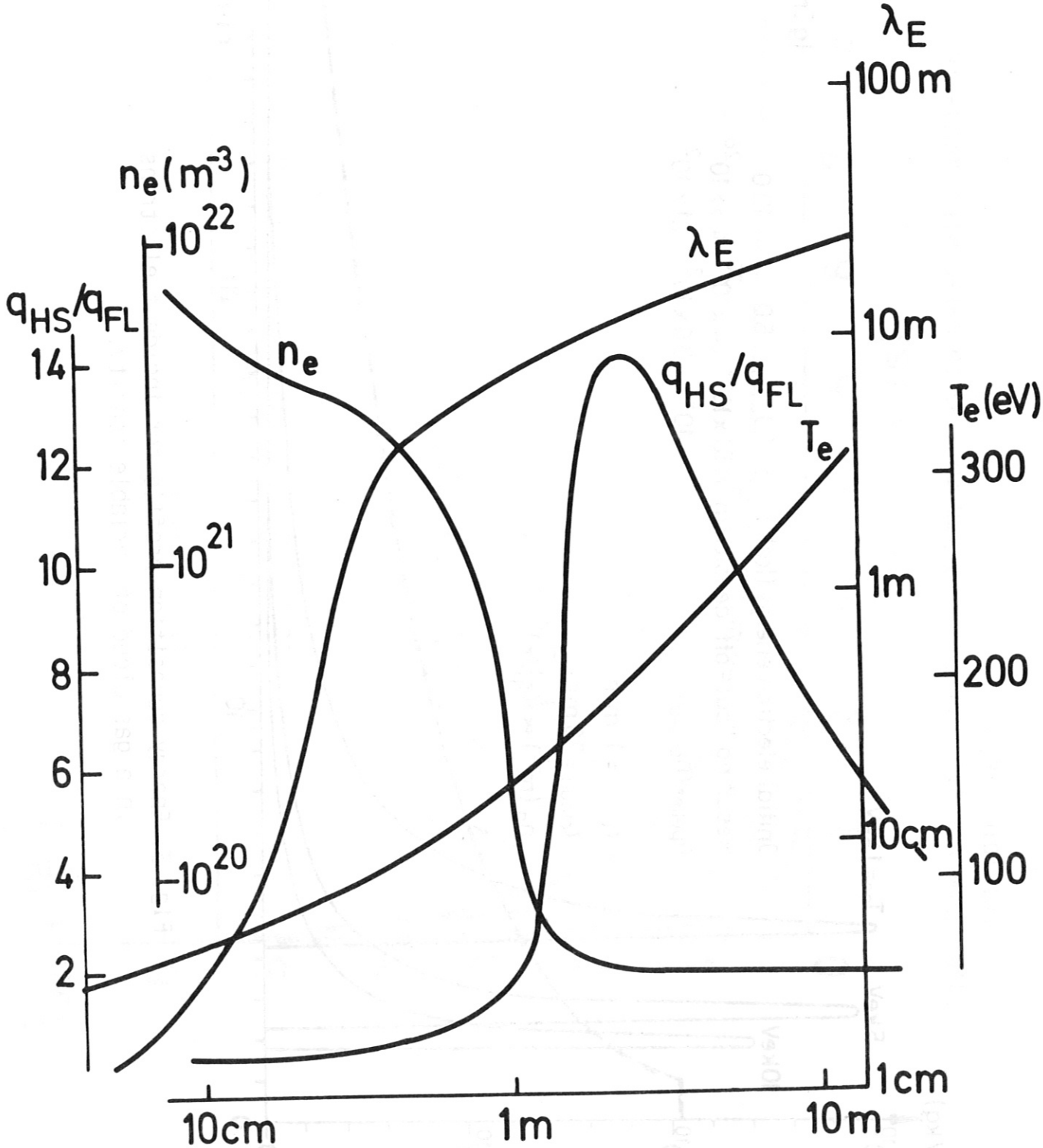

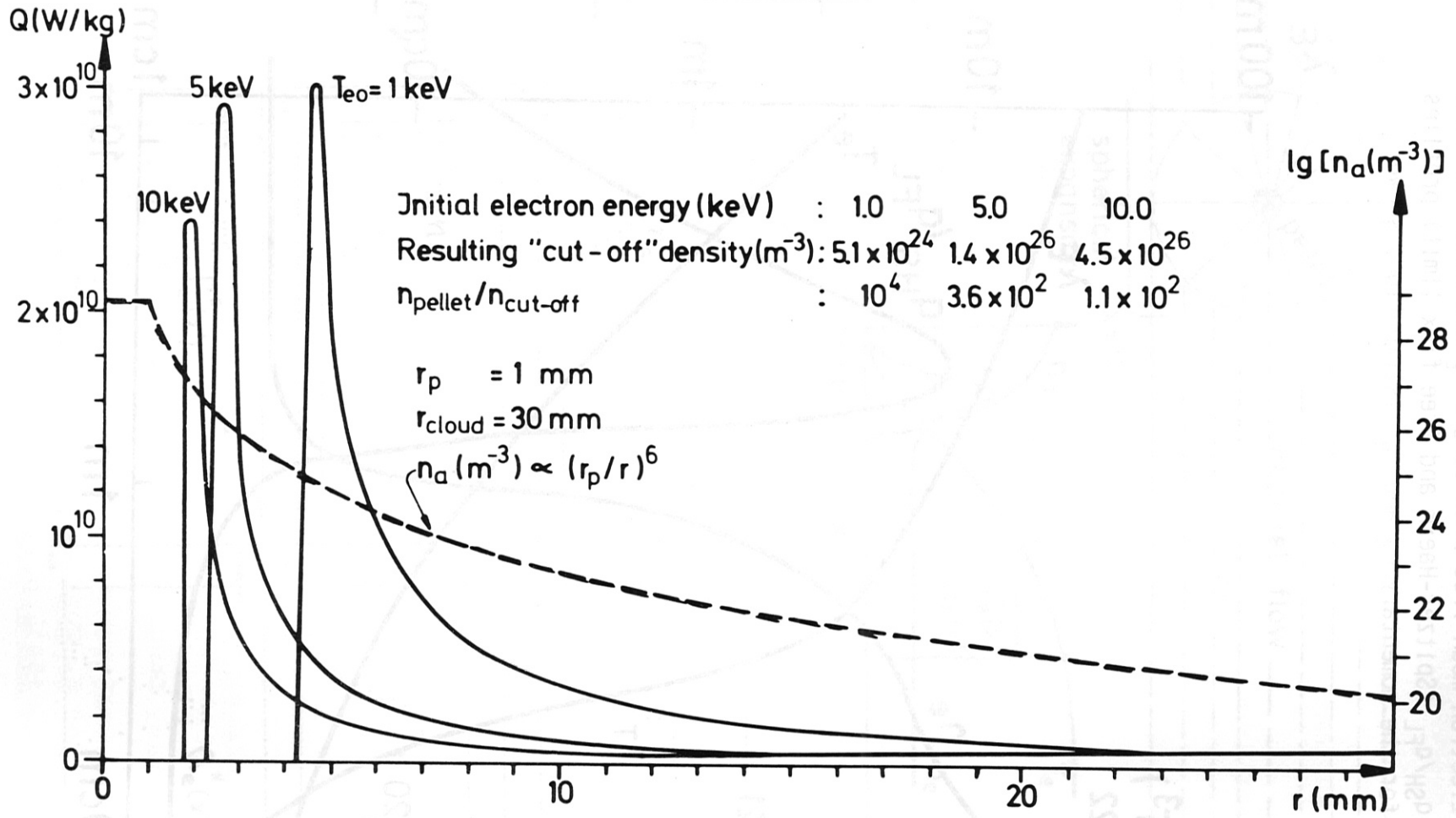

Fig. 3: Energy deposition profile for incident electrons in a gas cloud of variable density.

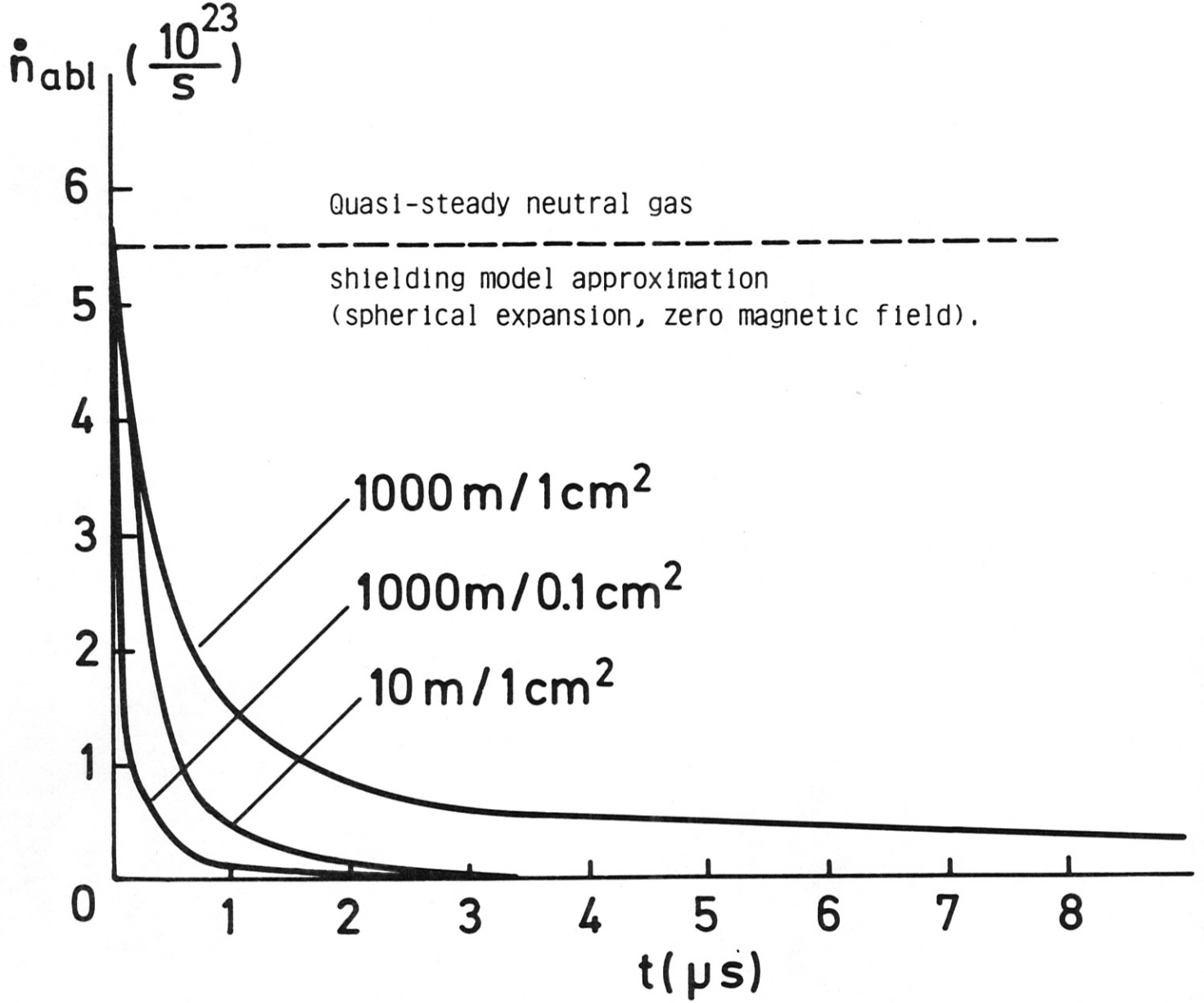

Fig.4: Time variation of the ablation rate as compared with quasi-steady neutral shielding value.